International Journal of Minerals, Metallurgy and Materials
Volume 27, Number 4, April 2020, Page 544
https://doi.org/10.1007/s12613-020-1975-6

Influence of glycine additive on corrosion and wear performance of electroplated trivalent chromium coating

Navid Mehdipour, Milad Rezaei, and Zeynab Mahidashti

Department of Materials and Metallurgical Engineering, Amirkabir University of Technology (Tehran Polytechnic), Hafez Ave., P.O. Box 15875-4413, Tehran, Iran

(Received: 24 May 2019; revised: 30 December 2019; accepted: 1 January 2020)

Abstract: The aim of this study is to evaluate the effect of various molar ratios of glycine to chromium salt (Gly : Cr) and different current densities on the corrosion and wear behaviors of Cr(III) electroplated coatings. The morphology and thickness of the coatings were investigated by scanning electron microscopy. The wear properties of the coatings were studied using pin on disk and hardness tests, while corrosion behavior of the coatings was identified using linear polarization, small amplitude cyclic voltammetry, and electrochemical impedance spectroscopy methods. By increasing the glycine concentration, a structure with low crack density was obtained. In all molar ratios, maximum thickness and current efficiency was observed at a current density of 150 $mA \cdot cm^{-2}$. All the electrochemical methods had a consistent result, and maximum corrosion resistance of approximately 16000 $\Omega \cdot cm^2$ was obtained in the case of Gly : Cr = 3:1 and current density of 200 $mA \cdot cm^{-2}$.

Keywords: electrodeposition; trivalent chromium; glycine; corrosion resistance

1. Introduction

Chromium coatings are typically used in the electroplating industry because of their special properties such as bright appearance, good wear resistance, and satisfactory corrosion behavior [1]. In common chromium electroplating methods, hexavalent chromium (Cr(VI)) bath is used, which has toxic and carcinogenic properties [2]. Therefore, trivalent chromium (Cr(III)) bath has been introduced as an alternative electrolyte because of its low toxicity [3−4]. However, several problems make the Cr(III) electroplating process extremely complex [5]. For instance, hexa-aqua complex $[Cr(H_2O)_6]^{3+}$ is formed through the entry of Cr(III) ion into water. In this case, Cr(III) in the center of the octahedral complex is surrounded by H_2O molecules, thereby hindering its reduction on the cathode surface [5−6]. Furthermore, during the Cr(III) electroreduction process, a considerable volume of H_2 gas is evolved as a result of the more negative reduction potential of Cr^{3+} (E^0 = −0.74 V vs. SHE (standard hydrogen electrode)) compared with that of H^+ (E^0 = –0.15 V vs. SHE at pH = 2.5). Hydrogen evolution reaction can lead to the development of micro and/or macro cracks in the chromium film and consequently reduce its corrosion resistance [6−8]. Moreover, if the local pH value on the cathode surface is increased to approximately 4 during the electroplating process, then H_2O molecules in the $[Cr(H_2O)_6]^{3+}$ complex can release hydrogen gas. Consequently, the chromium complexes are polymerized through hydroxyl ions, and long chains with heavy molecular weights are produced. This process, called olation or oxolation, decreases the deposition rate [6,9−11]. One way to overcome these problems is to introduce certain complexing agents to the electroplating bath, which can replace the H_2O molecules in the hexa-aqua complex, leading to easy reduction of Cr(III) ions. Consequently, these additives affect the current efficiency of the electroplating bath, surface structure, and corrosion behavior. Furthermore, bright appearance of the coating obtained is influenced by these additives [12]. Therefore, finding an appropriate material added to the Cr(III) electroplating bath to reach a desired corrosion performance and structure has been the focus of many studies [13−15].

Corresponding author: Milad Rezaei E-mail: miladrezaei@aut.ac.ir

Danilov *et al*. [16] examined the effect of a water-soluble polymer on the electroplating of chromium coatings from Cr(III)-based electrolytes; they reported a chromium coating with good adhesion to the surface, without cracks, and with a thickness of several tens of micrometer. Hoque *et al*. [17] investigated the effect of different additives such as polyethylene glycol and sodium sulfate on optical reflectivity of Cr(III) plated mild steel; their findings showed that the former increases reflectivity while the latter results in reduction of reflectivity. Protsenko *et al*. [18] reported a mechanism of chromium electrodeposition from methanesulfonate solutions of Cr(III) salts; they showed that electroreduction of Cr(III) ions proceed in a stepwise manner due to the formation of relatively stable Cr(II) intermediate compounds. Among various additives, glycine is reported to be a promising complexing agent in electroplating processes of various metals such as Ni and Co [19–22]. Glycine is used effectively in the electroplating of metals and alloys because of its buffering feature and its ability to stabilize pH value on the electrode surface during the electroplating process. Several reports also focus on the effect of glycine on the electroplating of Cr(III). For instance, Zeng *et al*. [14] studied the role of formic acid, oxalic acid, and glycine as complexing agents in a Cr(III) electroplating bath. Their results showed that glycine increases the distance between Cr(III) and H_2O molecules compared with the two others. Using density functional theory (DFT), the researchers demonstrated that glycine ions expand the distance between Cr^{3+} and H_2O from 0.199 nm in $[Cr(H_2O)_6]^{3+}$ to 0.2066 nm in $[Cr(H_2O)_4(H_2NCH_2COO)]^{+}$. However, to the best of our knowledge, no report is available on the corrosion behavior of the Cr(III) layer deposited from glycine-containing bath.

Therefore, considering the positive effects reported for glycine, this study aims to elucidate the effect of glycine additive and current density on the cathodic current efficiency of the chromium deposition, the thickness of the chromium deposits formed, and the corrosion behavior of the coatings obtained. Three independent electrochemical tests have been used to measure the polarization resistance of the coatings, i.e., linear polarization (LP), small amplitude cyclic voltammetry (SACV), and electrochemical impedance spectroscopy (EIS), to show the reliability of corrosion resistance quantities obtained from these three methods.

2. Methodology

2.1. Electroplating process

In this study, copper plates with dimensions of 8 cm × 2.5 cm were selected as substrates. Electroplating baths were prepared using analytical grade $CrCl_3 \cdot 6H_2O$ and glycine. Sodium hydroxide and hydrochloric acids were used for degreasing and pickling, respectively. For the electroplating process, the copper surface was polished mechanically by #1000 SiC emery paper (particle size: 18.3 μm) degreased with 1 $mol \cdot L^{-1}$ NaOH, rinsed by distilled water, activated in 18vol% HCl, and finally dried with air stream. To prepare the electroplating bath [19], the composition of which is given in Table 1, glycine and chromium salt with molar ratio of 1.5, 2, and 3 was used. The pH value of the electroplating bath was adjusted to 2.5 by addition of an appropriate amount of diluted NaOH and HCl. Then, solutions were heated at 80°C for 2 h and then were kept at room temperature for at least 24 h to ensure that the chromium complexes are formed. Electroplating was conducted at room temperature for 20 min at current densities of 100, 150, and 200 $mA \cdot cm^{-2}$. Two counter electrodes of Ti/IrO_2 with dimensions of 10 cm × 3.5 cm were selected as anode while copper plate was used as cathode (substrate). The reported results are related to the average of at least two electroplating process runs. For ease of referring to the coatings synthesized at different molar ratios of glycine to chromium salt (Gly : Cr) and current densities in the rest of the paper, the samples obtained are designated in the form of S (Gly : Cr molar ratio, current density), i.e., S (1.5, 100), S (1.5, 150), S (1.5, 200), S (2, 100), and so on.

Table 1. Chemical composition of electroplating solution $mol \cdot L^{-1}$

Solution	$CrCl_3 \cdot 6H_2O$	$C_2H_5NO_2$	NaCl	NH_4Cl	KBr	$AlCl_3 \cdot 6H_2O$	H_3BO_3
Gly : Cr = 1.5	0.4	0.6	0.5	0.5	0.08	0.01	0.5
Gly : Cr = 2	0.4	0.8	0.5	0.5	0.08	0.01	0.5
Gly : Cr = 3	0.4	1.2	0.5	0.5	0.08	0.01	0.5

2.2. Surface characterization

A Lega/Tescan-LMU scanning electron microscope (SEM) was used to study the surface morphology of the obtained coating. The thickness of the coatings was measured by Philips SEM with back-scattered electron beam. To prepare the cross sections, a square plate was cut from the corner of the electroplated samples by a mechanical cutter. Two edges of the corner, not touched by the cutter, were

available to be mounted and polished for subsequent SEM characterization. Each reported thickness is the average of three different points on the SEM micrograph. Wear properties was investigated by pin on disk test in which wear load and wear distance were set as 5 N and 200 m, respectively. Vickers microhardness was measured by a Micromet Buehler 60044. A 0.1-N load was applied on the top surface of the coatings for 15 s, and then hardness was reported as an average of three points on each sample.

2.3. Corrosion evaluation

To evaluate the steady-state corrosion properties of the coatings, the samples were immersed in 3.5wt% NaCl for 24 h before all the corrosion tests. Then, electrochemical tests were conducted in air saturated 3.5wt% NaCl solution, with an Autolab model PGSTAT 302N potentiostat/galvanostat in a three-electrode electrochemical cell (Ag/AgCl and Pt plates were used as reference and counter electrode, respectively). For LP test, a potential of ±100 mV vs. OCP (open circuit potential) at a scan rate of 1 $mV \cdot s^{-1}$ was applied, and the experimental data were fitted using OriginPro 8.6 software. EIS was conducted around the OCP in the frequency range of 10 kHz to 100 mHz. The value of peak-to-zero amplitude was ±10 mV. The obtained Nyquist diagrams were fitted on appropriate equivalent circuit by ZView software. SACV was carried out in a small potential range of ±10 mV around the OCP. The reported results are the average of two replicates.

3. Results and discussion

3.1. pH selection

The pH value is an important parameter in Cr(III) electroplating solution. When the pH value becomes greater than 4.5, the olation process occurs, thereby limiting the deposition of Cr(III) from aqueous solution. On the other hand, chromium oxides and hydroxides are deposited in the bath in high pH value. Thus, finding an optimum value for pH is important [8−11]. In this regard, the chromium stability in aqueous solution was plotted versus pH value by using Medusa software, as shown in Fig. 1. According to this plot, the Cr(III) ion is stable in the pH values lower than 2, so that aqua complex of Cr(III) ($[Cr(H_2O)_6]^{3+}$) is stable. In pH values greater than 3, the chromium oxide and hydroxide are stable. Therefore, the pH value of 2.5 was selected for the electroplating bath.

3.2. Current efficiency and appearance

The current efficiency (η) of the electroplating process was measured using the following equation:

$$\eta = \frac{m_{\text{real}}}{m_{\text{th}}} \times 100\% \quad (1)$$

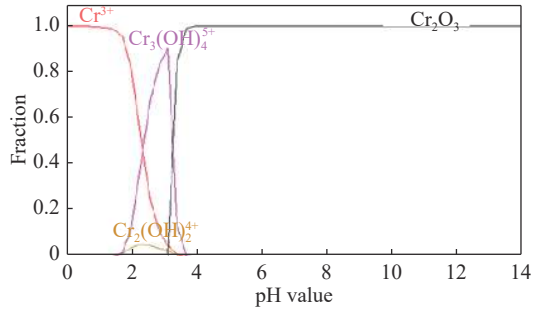

Fig. 1. Stability of Cr(III) contained complexes in aqueous solution vs. pH value for Cr total concentration of 0.4 $mol \cdot L^{-1}$, plotted by Medusa software.

where m_{real} is the mass gain of each sample after the electroplating process, while m_{th} is the theoretical mass calculated according to Faraday's law expressed as follows:

$$m_{\text{th}} = \frac{I \cdot M \cdot t}{Z \cdot F} \quad (2)$$

where I is the applied current (A), M is chromium molar mass ($g \cdot mol^{-1}$), t is electroplating time (s), Z is the number of exchange electrons, and F is Faraday's constant (96485 $C \cdot mol^{-1}$). Fig. 2 illustrates the results of estimated current efficiencies for different current densities and different Gly : Cr molar ratios. According to Fig. 2, by increasing the molar ratio of Gly : Cr in all current densities, the current efficiency is increased considerably. In the molar ratio of Gly : Cr = 3:1, the current efficiency exceeds 50%, whereas in Gly : Cr = 1.5:1, the current efficiency is less than 10%. It can be concluded that by adding glycine to the solution, a greater Cr−Gly complex is formed. In other words, in Gly : Cr = 1.5:1, the Cr(III) is more available in $[Cr(H_2O)_6]^{3+}$ form rather than Cr−Gly complex. As can be seen, in all cases,

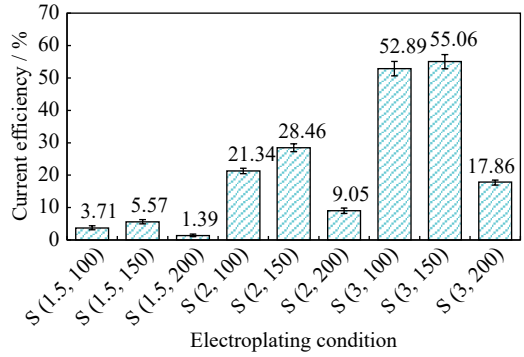

Fig. 2. Cathodic current efficiency obtained for coatings electroplated in different electroplating conditions.

the highest current efficiency is achieved by applying the current density of 150 mA·cm^{-2}. By increasing the current density to more than 150 mA·cm^{-2}, the hydrogen evolution reaction becomes more favorable than the reduction of Cr(III) ion so that the current efficiency is decreased. Another important point to mention is the appearance of the coatings, which have a reverse relation with glycine amount, i.e., the semi-bright coatings were obtained in baths with low molar ratio of Gly : Cr. The coating appearance is demonstrated in Fig. 3.

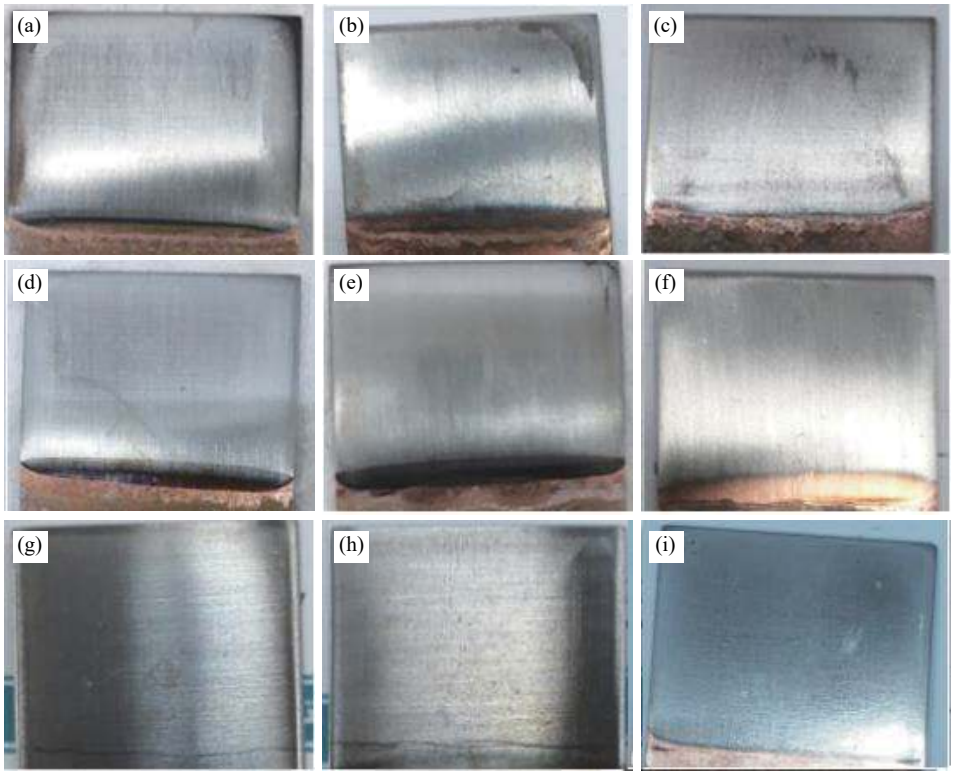

Fig. 3. Appearance of coatings electroplated in different electroplating conditions: (a) S (1.5, 100); (b) S (1.5, 150); (c) S (1.5, 200); (d) S (2, 100); (e) S (2, 150); (f) S (2, 200); (g) S (3, 100); (h) S (3, 150); (i) S (3, 200).

3.3. Surface properties

Fig. 4 shows the SEM micrographs of chromium coating surface after electroplating in different current densities and molar ratios of Gly : Cr. As the figure shows, a denser surface layer is formed in samples with molar ratio of Gly : Cr = 3:1 (Figs. 4(c), 4(f), and 4(i)) compared with that with molar ratio of Gly : Cr = 2:1 (Figs. 4(b), 4(e) and 4(h)) and 1.5:1 (Figs. 4(a), 4(d) and 4(g)). This result again confirms the effective role of glycine in the formation of Cr−glycine complex, favoring the enhanced formation of chromium film. With regard to current density, the degree of compactness is increased by raising the current density so that the structure in 100 mA·cm^{-2} is practically porous with some macro cracks, whereas the number of grains is decreased in 200 mA·cm^{-2} and some micro cracks with almost no cavity are formed in the coatings.

The cross-section structure and thickness of the coatings were also studied by SEM, and the micrographs and values of the coating thickness are reported in Fig. 5. As the figure shows, several cracks occur in the cross section of the coatings and some of these cracks have reached the substrate, thereby reducing the corrosion resistance of the electroplated chromium coatings, as will be discussed in the next section. By increasing the glycine concentration in the solution, the coating thickness increases and the maximum thickness is obtained at current density of 150 mA·cm^{-2} in all the solutions. These results are in accordance with the data obtained in the current efficiency section.

The wear behavior of the electroplated coatings with highest thickness in the solution with different molar ratios of Gly : Cr, i.e., S (2, 150) and S (3, 150), were compared using pin-on-disk test. The results are shown in Fig. 6 as friction coefficient versus wear distance (S (1, 150) was not tested because of low thickness). In both samples, the fric-

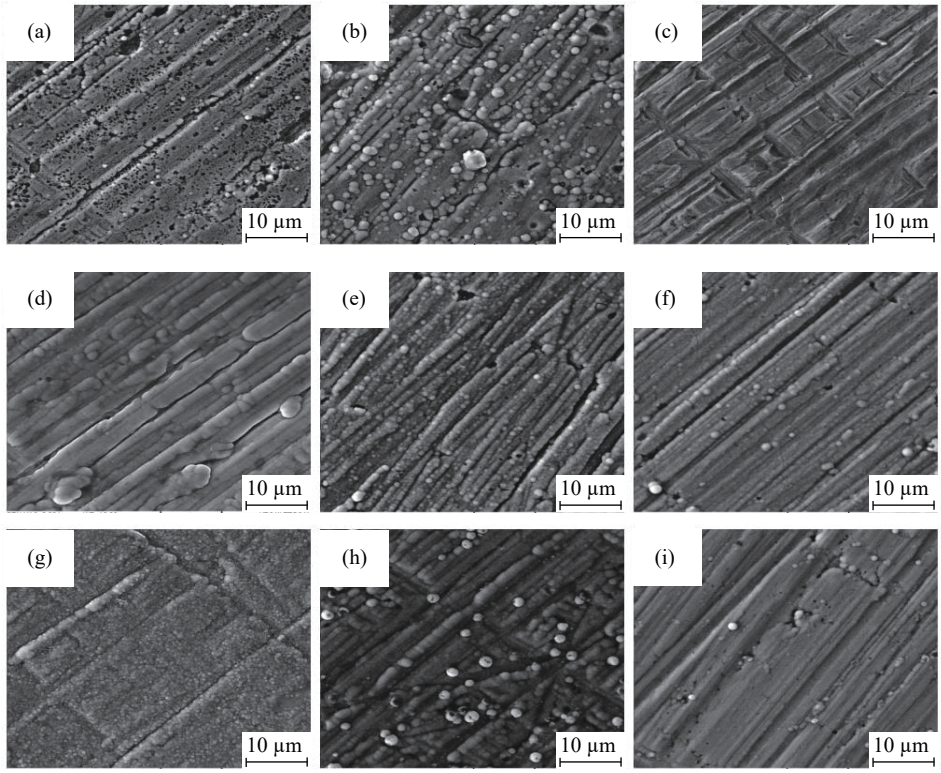

Fig. 4. SEM images of coatings electroplated in different electroplating conditions: (a) S (1.5, 100); (b) S (1.5, 150); (c) S (1.5, 200); (d) S (2, 100); (e) S (2, 150); (f) S (2, 200); (g) S (3, 100); (h) S (3, 150); (i) S (3, 200).

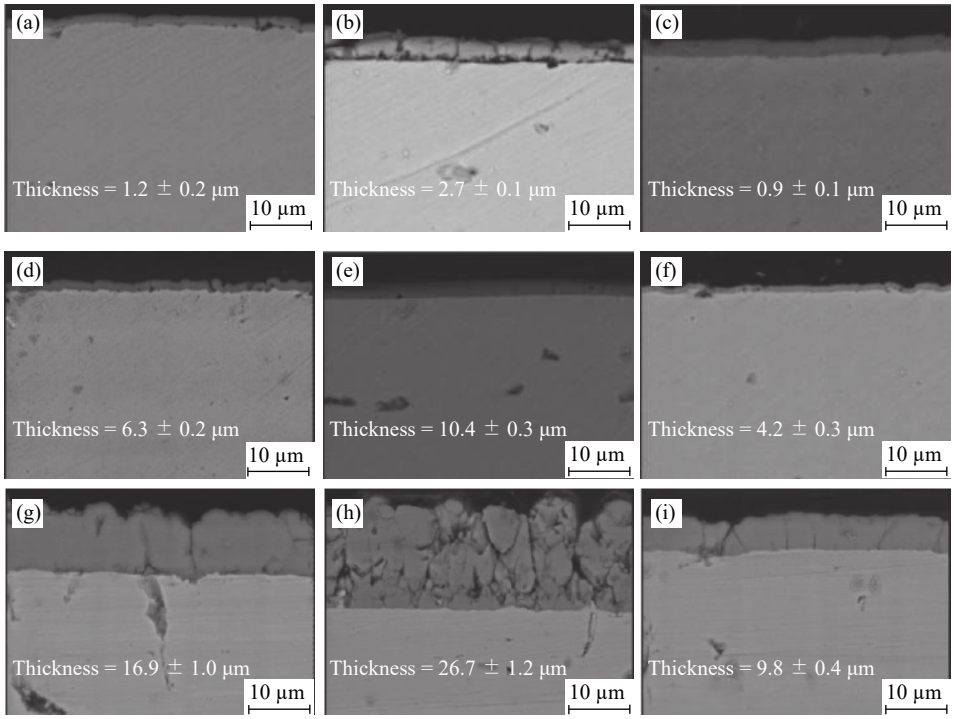

Fig. 5. SEM back-scattered micrographs of cross section of Cr(III) coatings electroplated in different electroplating conditions: (a) S (1.5, 100); (b) S (1.5, 150); (c) S (1.5, 200); (d) S (2, 100); (e) S (2, 150); (f) S (2, 200); (g) S (3, 100); (h) S (3, 150); (i) S (3, 200).

tion coefficient is first increased and becomes approximately constant after reaching a peak. In the graph related to the coating electroplated in a solution with molar ratio of Gly : Cr = 2:1, the friction coefficient is approximately 0.25,

which increases to 0.4 and then approaches 0.3 until the end of the wear distance. In the graph related to the molar ratio of Gly : Cr = 3:1, the friction coefficient is approximately 0.2, which increases to the sharp peak equal to 0.5 and then approaches 0.3. The cause of an initial increase in friction coefficient is the rise of surface temperature during the movement of the pin on the coat. Thereafter, the counterpart matches the coat surface and the friction coefficient reaches an approximately constant value. The data obtained from the hardness test show that S (2, 150) and S (3, 150) have a hardness of HV 794 and HV 864, respectively. These results are in line with the friction coefficient values obtained because the real contact area between the samples and ball decreases with the increase in hardness. Thus, the coefficient of friction is reduced. The specific wear rate of the two coatings under wear test is reported in Fig. 6. The coating obtained in molar ratio of Gly : Cr = 3:1 solution has lower specific wear rate than the coating obtained in molar ratio of Gly : Cr = 2:1. On the other hand, wear resistance has a direct relationship with hardness of material according to Archard theory [23]. Therefore, the lower specific wear rate of S (3, 150) can be attributed to the higher hardness observed in this sample.

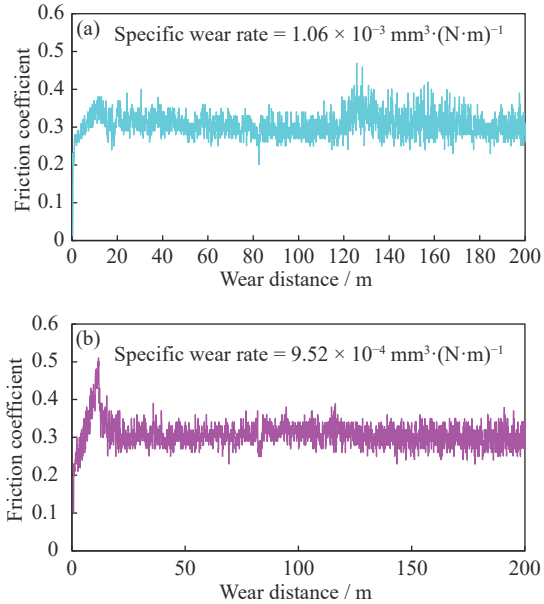

Fig. 6. Friction coefficient vs. wear distance and specific wear rate obtained from pin on disk test with 5 N applied load conducted on (a) S (2, 150) and (b) S (3, 150).

3.4. Corrosion behavior

3.4.1. Linear polarization (LP)

Fig. 7 shows the polarization curves obtained for electroplated chromium coatings in air saturated 3.5wt% NaCl solution. Although the Tafel extrapolation method is frequently used for extracting the corrosion parameters including E_{corr} (i.e. corrosion potential), i_{corr} (i.e. corrosion current constant), β_a (i.e. anodic Tafel constant), and β_c (i.e. cathodic Tafel constant), this method has certain limitations [24]. Therefore, the Butler–Volmer equation (Eq. (3)) [25] was fitted non-linearly on $i-E$ curves by using OriginPro 8.6 software and the corrosion parameters for all samples were extracted using this fitting. The results are reported in Table 2 and a typical fitted plot is shown in Fig. 8 for S (3, 200). To verify the accuracy of the fitting, polarization resistance (R_p) was calculated according to the Stern–Geary equation (Eq. (4)) using the corrosion parameters obtained and was compared with the R_p estimated according to the slope of the linear polarization curve around the corrosion potential (Eq. (5)). A typical estimation is shown in Fig. 9 for S (3, 200). As shown in the results reported in Table 2, good consistency exists between the R_p values calculated by the Stern–Geary equation (R_p (S–G)) and the R_p values obtained by the slope of the $i-E$ curve (R_p (LP)), which confirms the correctness of the non-linear fitting procedure on experimental data and the corrosion parameters obtained.

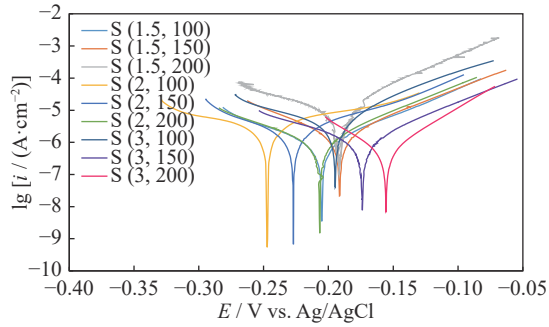

Fig. 7. Linear polarization curves of electroplated chromium coatings in air saturated 3.5wt% NaCl solution. The applied potential is ±100 mV versus E_{corr}, the scan rate is 1 mV/s, and the immersion time for each sample is 24 h.

$$i = i_{corr} \times \left\{ \exp\left[\left(\frac{2.303}{\beta_\alpha}\right) \times (E - E_{corr})\right] - \exp\left[\left(\frac{-2.303}{\beta_c}\right) \times (E - E_{corr})\right] \right\} \quad (3)$$

$$R_p = \frac{\beta_a \times \beta_c}{2.303 \times (\beta_a + \beta_c)} \times \frac{1}{i_{corr}} \quad (4)$$

$$R_p = \frac{\Delta E}{\Delta i} \quad (5)$$

where E (V) is potential applied and i (A·cm^{-2}) is current obtained during polarization test.

As shown in the Table 2, S (3, 200) has the greatest polarization resistance whereas S (1.5, 200) has the lowest res-

istance. According to Fig. 5, the former has a thickness of 9.8 μm, while the latter's thickness is only 0.9 μm. Both samples have been electroplated with the same current density but different amounts of glycine. Thus, it can be said that a suitable amount of glycine within the electroplating bath has been introduced into the $[Cr(H_2O)_6]^{3+}$ complex and replaced with H_2O molecules, thereby resulting in $[Cr(H_2O)_{6-n}G_n]^{3-n}$ complex formation (G is glycine ligand). This condition increases the distance between Cr(III) and H_2O molecules within the complex, which facilitates the electrochemical reduction of Cr(III) on the substrate; thus, the thickness increases [5,14,26]. On the other hand, by comparing the samples electroplated with the same amount of molar ratio of Gly : Cr = 3:1 but different current densities, it can be observed that the corrosion resistance increases by raising the current density. According to the current efficiency data, the amount of current allocated to the Cr deposition in 100 or 150 $mA·cm^{-2}$ current densities is much higher than that at 200 $mA·cm^{-2}$ so that a thicker coating is deposited in S (3,100) and S (3,150) compared with S (3, 200). However, in these cases, the deposited layer has a high amount of porosities and cracks, which opens up the path for corrosive ion attacks and leads to the reduction of corrosion resistance. These cracks result from residual tensile stress produced by grain boundary misfits, which are intensified by the increment of allocated current [27].

Table 2. Corrosion parameters obtained by non-linear fitting of Butler–Volmer equation on the experimental data, R_p values obtained according to Stern–Geary equation (R_p (S–G)), slope of linear region of i–E plot (R_p (LP)) and SACV test (R_p (SACV)), and corrosion rate (C.R.) calculated by Faraday's law

Sample	i_{corr} / ($\mu A·cm^{-2}$)	E_{corr} / V vs. Ag/AgCl	β_a / ($V·dec^{-1}$)	β_c / ($V·dec^{-1}$)	R_p (LP) / ($\Omega·cm^2$)	R_p (S–G) / ($\Omega·cm^2$)	R_p (SACV) / ($\Omega·cm^2$)	C.R. / ($\mu m·a^{-1}$)
S (1.5, 100)	2.75	−0.205	0.0861	0.1083	7466	7572	5920	21.8
S (1.5, 150)	2.48	−0.191	0.0786	0.0968	7567	7592	7622	19.7
S (1.5, 200)	6.15	−0.191	0.0432	0.0500	1525	1637	5857	48.8
S (2, 100)	15.70	−0.247	0.4134	0.5796	5386	6692	5709	124.7
S (2, 150)	8.93	−0.227	0.2014	0.5340	7060	7110	7716	70.9
S (2, 200)	3.45	−0.206	0.1269	0.3898	11868	11934	9171	27.4
S (3, 100)	5.16	−0.194	0.0565	0.1562	3359	3489	3162	41.0
S (3, 150)	4.18	−0.173	0.1538	0.4998	11994	12227	10952	33.2
S (3, 200)	0.73	−0.160	0.0487	0.0599	15909	15956	14284	5.8

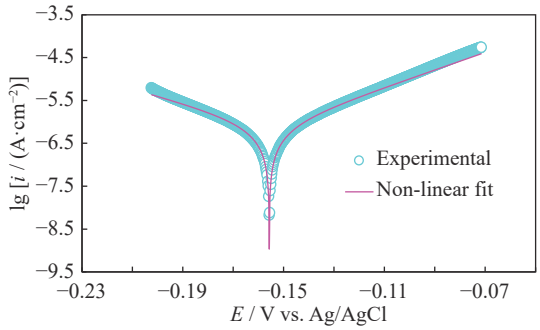

Fig. 8. Non-linear fitted polarization curve based on Butler–Volmer equation around E_{corr} for S (3, 200).

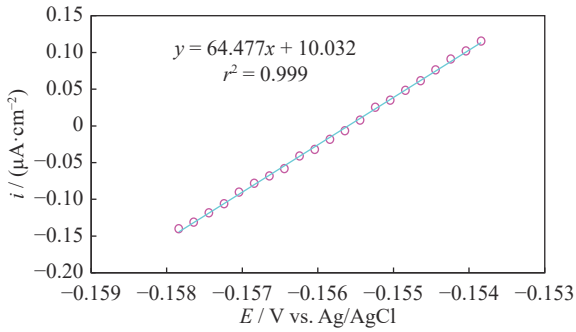

Fig. 9. Typical i–E plot in the range of ±15 mV around OCP for S (3, 200) to calculate R_p from the slope of the curve.

Another important parameter is the corrosion potential, E_{corr}, which has the least negative value for the sample with lowest corrosion rate and the most negative value for that with the highest corrosion rate. The least negative value of the corrosion potential is due to the reduction in the rate of anodic reaction due to the formation of a homogeneous passive chromium film on the substrate [28].

Furthermore, all the polarization curves are similar in the shape of the anodic and cathodic branches, showing a similar mechanism for corrosion reactions. As shown in Table 2, S (3,200) has the lowest β_a and β_c besides E_{corr}. Tafel constants are indicators of the share of cathodic and anodic reactions. The homogenous passive film formed on the mentioned sample can hinder cathodic and anodic reactions on the sample to a great extent.

Furthermore, the corrosion rate of the coatings in terms of $\mu m·a^{-1}$ unit is calculated according to Faraday's law (Eq. 6) and is reported in Table 2.

$$\text{C.R.} = \frac{3.27 \times M \times i_{corr}}{\rho \times Z} \tag{6}$$

where ρ is the density of chromium ($g·cm^{-3}$), M is the molar

weight of chromium (g·mol^{-1}), and i_{corr} is the corrosion current density (μA·cm^{-2}).

All of the calculated corrosion rates are lower than 125 μm·a^{-1}, categorizing these coatings as excellent according to Fontana's classification [24].

3.4.2. Small amplitude cyclic voltammetry (SACV)

Another test used for independent measurement of the polarization resistance (R_p), was SACV. According to the analysis by Macdonald [29], a new parameter called R_d can be calculated as follows:

$$\frac{1}{R_d} = \frac{1}{R_p + R_s} + \frac{2R_p^2 C\left(e^{\frac{aE_m}{vb}} - 1\right)v}{E_m\left(R_p + R_s\right)^2\left(e^{\frac{aE_m}{vb}} + 1\right)} \quad (7)$$

where R_d is diagonal resistance (Ω·cm^2), R_s is solution resistance (Ω·cm^2), R_p is polarization resistance (Ω·cm^2), v is potential scan rate (V·s^{-1}), C is interfacial capacitance (F·cm^{-2}), $a = R_p + R_s$, and $b = R_sR_pC$. A potentiostatic cyclic voltammetry technique is selected for plotting the i–E curve in a conventional three-electrode electrochemical cell contained air saturated 3.5wt% NaCl solution. The i–E curves are plotted in the range of ±10 mV around the OCP. The test is repeated in different scan rates changed from 10 to 5, 1, 0.9, 0.8, 0.7, 0.6, 0.5, 0.4, 0.3, 0.2, and 0.1 mV·s^{-1}. These cyclic curves are shown in Fig. 10 for S (3, 200). For each cycle, the slope of the line between maximum and minimum potential is recorded as in Fig. 11(a), which is equal to R_d^{-1}. At the end, R_d^{-1} vs. v is plotted and extrapolated to zero scan rate (Fig. 11(b)) [24]. According to Eq. (7), R_d approaches $R_p + R_s$ when v approaches zero; thus, the intercept of R_d^{-1} –v plot equals to $(R_p + R_s)^{-1}$. On the other hand, R_s can be measured by using a conductivity meter. Special conductivity (Γ) of air saturated 3.5wt% NaCl was measured at 45 mS·cm^{-1} and in the three-electrode cell, the distance between reference and working electrode (l) was 0.5 cm. Thus, according to Eq. (8), R_s can be estimated at approximately 11 Ω·cm^2.

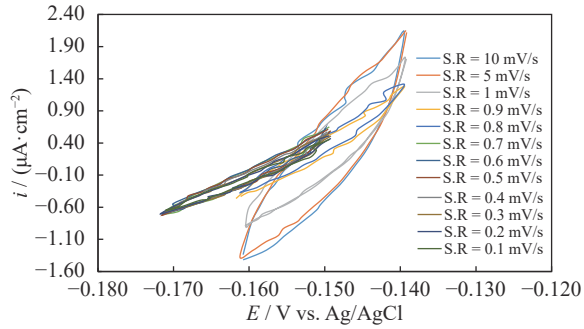

Fig. 10. A typical polarization curve plotted as SACV for S (3, 200) in air saturated 3.5wt% NaCl in the potential range of ±10 mV with respect to OCP at different scan rates. S.R means scan rate.

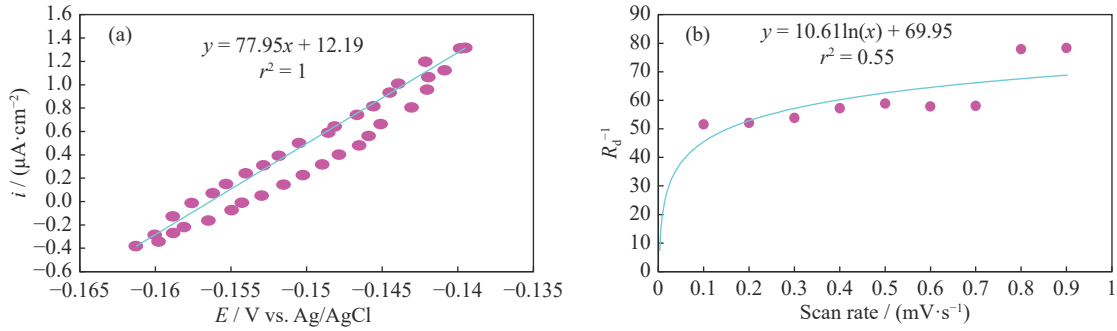

Fig. 11. (a) Calculation of R_d from SACV; (b) 1/R_d as a function of scan rate and logarithmic trend for extrapolating to zero scan rate. The marker points and solid lines correspond to the experimental data and extrapolation results.

$$R_s = \frac{l}{\Gamma} \quad (8)$$

These steps are repeated for all the coatings and the recorded R_p is demonstrated in Table 2. In the SACV test, the maximum polarization resistance corresponds to S (3, 200) and the minimum value belongs to this bath with plating current density of 100 mA·cm^{-2}, which is in line with previous results. This result means that the morphology of the coatings becomes less cracked as the current density increases. In the bath with molar ratio of Gly : Cr = 3:1 compared with molar ratio of Gly : Cr = 2:1 and 1.5:1 at current density of 150 mA·cm^{-2}, the polarization resistance of the coatings increased because a larger amount of Cr(III)–glycine complex is available and the coating with a compact structure is formed. These results are in accordance with those obtained from the previous test.

3.4.3. Electrochemical impedance spectroscopy (EIS)

The results of EIS test for Cr(III) coatings are displayed as Nyquist and Bode diagrams in Fig. 12. From the Bode phase diagram, only one peak and therefore, only one time

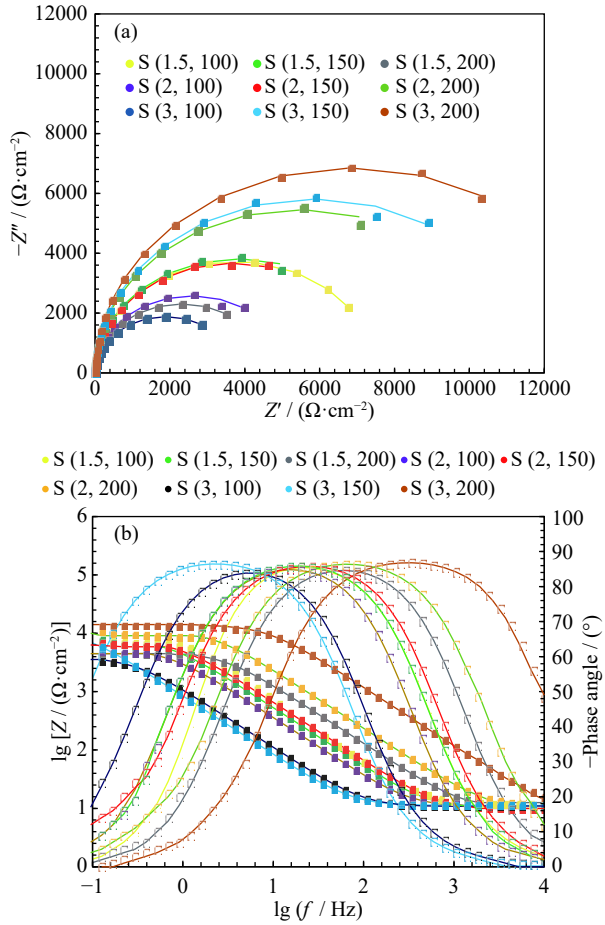

Fig. 12. Nyquist (a) and Bode (b) diagrams for Cr(III) coatings in air saturated 3.5wt% NaCl in the frequency range of 100 mHz–10 kHz. The marker points and solid lines correspond to the experimental data and fitted results, respectively. Filled and hollow marker points correspond to lg(Z) and –phase angle axes, respectively.

constant can be observed. In other words, only one electrode/electrolyte interface exists in the corroding system. This behavior was also observed by other researchers [3,5,30−31]. The diameter of the semi-circle of the Nyquist diagram indicates the charge transfer resistance that can be considered as R_p when no pseudo-inductive behavior is present in the system [32]. As shown in Fig.12(a), S (3, 200) has the largest while S (3, 100) has the smallest diameter. Furthermore, the Nyquist plot obtained is a depressed circle rather than a perfect one in some cases. The reason is that in most corrosion phenomena, a constant phase element is present in the system instead of a capacitor due to the frequency dispersion effect caused by several factors, such as roughness and surface inhomogeneities [5]. Accordingly, the equivalent circuit used for fitting the data is a one-time constant Randles circuit shown in Fig. 13 and the extracted data are reported in Table 3. In this equivalent circuit, R_s is the resistance of air saturated with 3.5wt% NaCl, R_p is the polarization resistance, and CPE is the constant phase element, the impedance of which (Z_{CPE}) is given as follows:

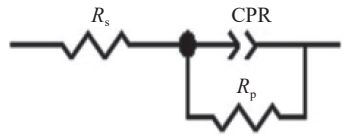

Fig. 13. Electrical equivalent circuit for fitting the Nyquist diagram.

$$Z_{CPE} = 1/(Y_0(j\omega)^n) \quad (9)$$

where ω is angular frequency (rad·s^{-1}) and Y_0 (admittance) is constant of CPE (s^n·Ω^{-1}·cm^{-1}), which has a direct relation with the active surface area exposed to the electrolyte and n is power number of CPE.

According to the proposed circuit, the impedance of the system (Z) can be calculated as follows:

$$Z = R_s + \frac{1}{\frac{1}{R_p} + Y_0(j\omega)^n} \quad (10)$$

At high frequency range (high ω), the obtained impedance is equal to R_s. From the Bode plots (Fig. 12(b)), it can be observed that lg|Z| at high frequency has the same value for all the coatings. R_s depends on the distance between the

Table 3. Estimated parameters obtained from impedance plots of different samples exposed to 3.5wt% NaCl solution at room temperature

Sample	R_s / (Ω·cm^2)	Y_0 / (s^n·Ω^{-1}·cm^{-1})	n	R_p / (Ω·cm^2)
S (1.5, 100)	11.8	2.59×10^{-6}	1	7467
S (1.5, 150)	10.3	2.97×10^{-5}	1	7624
S (1.5, 200)	10.2	1.22×10^{-5}	0.99	4612
S (2, 100)	10.8	4.38×10^{-5}	1	5140
S (2, 150)	9.8	2.41×10^{-5}	0.99	7339
S (2, 200)	11.2	6.74×10^{-6}	1	10907
S (3, 100)	10.8	1.43×10^{-4}	1	3759
S (3, 150)	11.3	1.87×10^{-4}	1	11626
S (3, 200)	10.5	1.34×10^{-6}	0.99	13714

reference and working electrodes. This distance was kept approximately constant during all the tests. Therefore, the values obtained for R_s is approximately constant and around 11 $\Omega \cdot cm^2$, as shown in Table 3.

At low frequency, however, the impedance of the CPE tends to zero and circuit impedance becomes equal to $R_s + R_p$. As shown by the Bode plot, S (3, 200) has the highest R_p. Furthermore, according to Table 3, this coating has the lowest Y_0 value of 1.34×10^{-6}, which indicates minimum cracks and active surface area within the coating for corrosion reactions to take place. These results confirm superior barrier and corrosion performance of the sample synthesized at 200 $mA \cdot cm^{-2}$ using glycine-to-chromium molar ratio of 3.

Most of the R_p values obtained by EIS test are in accordance with the LP and SACV test as reported in Fig. 14. In most cases, an acceptable consistency can be observed among the results obtained from the LP, SACV, and EIS tests, which indicates the acceptable accuracy of the corrosion tests performed.

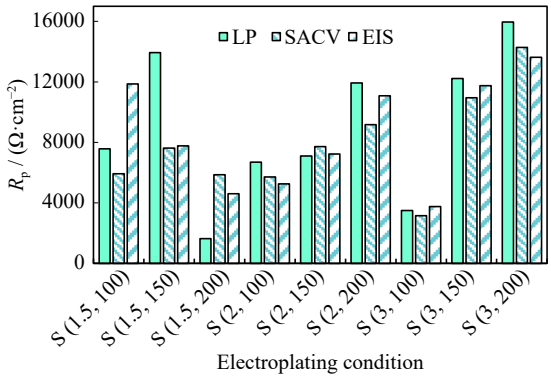

Fig. 14. Comparison among corrosion resistance (R_p) obtained by three independent tests, including linear polarization test (LP), small amplitude cyclic voltammetry (SACV), and electrochemical impedance spectroscopy (EIS).

4. Conclusions

(1) The coating with favorable appearance was obtained by using glycine as a complexing agent in Cr(III) bath and pH equal to 2.5.

(2) The best wear behavior was observed in the case of molar ratio of Gly : Cr = 3:1 and current density of 150 $mA \cdot cm^{-2}$. In the mentioned condition, a thickness of 26.7 μm, chathodic current efficiency of 55.06%, and a hardness of HV 864 was obtained. The lowest weight loss belonged to the coatings electroplated by this solution.

(3) The corrosion resistance of chromium coatings was measured by three independent tests (LP, SACV, and EIS). The maximum R_p was approximately equal to 16000 $\Omega \cdot cm^2$, which was related to coatings electroplated in a solution with the molar ratio of Gly : Cr = 3:1 and current density of 200 $mA \cdot cm^{-2}$. This result demonstrates that the corrosion resistance is affected by morphology and cracks continued to the substrate. The values of polarization resistance obtained from three independent tests showed good consistency, which ensures the accuracy of the corrosion tests.

References

[1] K.S. Nam, K.H. Lee, S.C. Kwon, D.Y. Lee, and Y.S. Song, Improved wear and corrosion resistance of chromium(III) plating by oxynitrocarburising and steam oxidation, *Mater. Lett.*, 58(2004), No. 27-28, p. 3540.

[2] Z. Mahidashti, M. Aliofkhazraei, and N. Lotfi, Review of nickel-based electrodeposited tribo-coatings, *Trans. Indian Inst. Met.*, 71(2018), No. 2, p. 257.

[3] G. Saravanan and S. Mohan, Corrosion behavior of Cr electrodeposited from Cr(VI) and Cr(III)-baths using direct (DCD) and pulse electrodeposition (PED) techniques, *Corros. Sci.*, 51(2009), No. 1, p. 197.

[4] N. Van Phuong, S.C. Kwon, J.Y. Lee, J.H. Lee, and K.H. Lee, The effects of pH and polyethylene glycol on the Cr(III) solution chemistry and electrodeposition of chromium, *Surf. Coat. Technol.*, 206(2012), No. 21, p. 4349.

[5] H.A. Ramezani-Varzaneh, S.R. Allahkaram, and M. Isakhani-Zakaria, Effects of phosphorus content on corrosion behavior of trivalent chromium coatings in 3.5wt% NaCl solution, *Surf. Coat. Technol.*, 244(2014), p. 158.

[6] R. Giovanardi and G. Orlando, Chromium electrodeposition from Cr(III) aqueous solutions, *Surf. Coat. Technol.*, 205(2011), No. 15, p. 3947.

[7] N.V. Mandich, Chemistry and theory of chromium deposition: Part 1: chemistry, *Plat. Surf. Finish.*, 84(1997), No. 5, p. 108.

[8] M. Vidal, M. Ostra, N. Imaz, E. García-Lecina, and C. Ubide, Analysis of SEM digital images to quantify crack network pattern area in chromium electrodeposits, *Surf. Coat. Technol.*, 285(2016), p. 289.

[9] S. Survilienė, O. Nivinskienė, A. Češunienė, and A. Selskis, Effect of Cr(III) solution chemistry on electrodeposition of chromium, *J. Appl. Electrochem.*, 36(2006), No. 6, p. 649.

[10] E.S.C. Ferreira, C.M. Pereira, and A.F. Silva, Electrochemical studies of metallic chromium electrodeposition from a Cr(III) bath, *J. Electroanal. Chem.*, 707(2013), p. 52.

[11] S.L. Handy, C.F. Oduoza, and T. Pearson, Theoretical aspects of electrodeposition of decorative chromium from trivalent electrolytes and corrosion rate study of different nickel/chromium coatings, *Trans. IMF*, 84(2006), No. 6, p. 300.

[12] C.A. Huang, W. Lin, and M.J. Liao, The electrochemical behavior of the bright chromium deposits plated with direct- and pulse-current in 1 M H_2SO_4, *Corros. Sci.*,

48(2006), No. 2, p. 460.
[13] C.E. Lu, N.W. Pu, K.H. Hou, C.C. Tseng, and M.D. Ger, The effect of formic acid concentration on the conductivity and corrosion resistance of chromium carbide coatings electroplated with trivalent chromium, *Appl. Surf. Sci.*, 282(2013), p. 544.
[14] Z.X. Zeng, Y.X. Zhang, W.J. Zhao, and J.Y. Zhang, Role of complexing ligands in trivalent chromium electrodeposition, *Surf. Coat. Technol.*, 205(2011), No. 20, p. 4771.
[15] Z.X. Zeng, L.P. Wang, A.M. Liang, and J.Y. Zhang, Tribological and electrochemical behavior of thick Cr–C alloy coatings electrodeposited in trivalent chromium bath as an alternative to conventional Cr coatings, *Electrochim. Acta*, 52(2006), No. 3, p. 1366.
[16] F.I. Danilov, V.S. Protsenko, T.E. Butyrina, E.A. Vasil'eva, and A.S. Baskevich, Electroplating of chromium coatings from Cr(III)-based electrolytes containing water soluble polymer, *Prot. Met.*, 42(2006), No. 6, p. 560.
[17] Md.A. Hoque, M.E. Haque, Md.M. Islam, Md.S. Islam, and C.M. Mustafa, Electroplating of chromium from Cr(III) aqueous solutions on the mild steel: Optimization of bath constituents, *Int. J. Innovation Sci. Math.*, 3(2015), No. 2, p. 124.
[18] V.S. Protsenko, A.A. Kityk and F.I. Danilov, Kinetics and mechanism of chromium electrodeposition from methanesulfonate solutions of Cr(III) salts, *Электронная обработка материалов*, 50(2014), No. 5, p. 13.
[19] A. Baral and R. Engelken, Modeling, optimization, and comparative analysis of trivalent chromium electrodeposition from aqueous glycine and formic acid baths, *J. Electrochem. Soc.*, 152(2005), No. 7, p. C504.
[20] İ.H. Karahan, Effects of pH value of the electrolyte and glycine additive on formation and properties of electrodeposited Zn–Fe coatings, *Sci. World J.*, 2013(2013), art. No 273953.
[21] R.A.J. Critelli and P.T.A. Sumodjo, Influence of glycine as additive on cobalt electrodeposition, *ECS Trans.*, 50(2013), No. 52, p. 75.
[22] M.A.M. Ibrahim and R.M. Al Radadi, Role of glycine as a complexing agent in nickel electrodeposition from acidic sulphate bath, *Int. J. Electrochem. Sci.*, 10(2015), p. 4946.
[23] J.F. Archard, Contact and rubbing of flat surfaces, *J. Appl. Phys.*, 24(1953), No. 8, p. 981.
[24] M.G. Fontana, *Corrosion Engineering*, 3rd, McGraw-Hill Company, New York, 1987, p. 172.
[25] A.J. Bard, L.R. Faulkner, J. Leddy, and C.G. Zoski, *Electrochemical Methods: Fundamentals and Applications*, Wiley, New York, 1980.
[26] F.A. Lowenheim and J. Davis, Modern electroplating, *J. Electrochem. Soc.*, 121(1974), No. 12, p. 397C.
[27] C. Bergenstof Nielsen, P. Leisner, and A. Horsewell, On texture formation of chromium electrodeposits, *J. Appl. Electrochem.*, 28(1998), No. 2, p. 141.
[28] S. Yagi, A. Sengoku, K. Kubota, and E. Matsubara, Surface modification of ACM522 magnesium alloy by plasma electrolytic oxidation in phosphate electrolyte, *Corros. Sci.*, 57(2012), p. 74.
[29] D.D. Macdonald, An impedance interpretation of small amplitude cyclic voltammetry I. Theoretical analysis for a resistive-capacitive system, *J. Electrochem. Soc.*, 125(1978), No. 9, p. 1443.
[30] A. Sheibani Aghdam, S.R. Allahkaram, and S. Mahdavi, Corrosion and tribological behavior of Ni–Cr alloy coatings electrodeposited on low carbon steel in Cr(III)–Ni (II) bath, *Surf. Coat. Technol.*, 281(2015), p. 144.
[31] G. Saravanan and S. Mohan, Pulsed electrodeposition of microcrystalline chromium from trivalent Cr-DMF bath, *J. Appl. Electrochem.*, 39(2009), No. 8, p. 1393.
[32] M. Lebrini, G. Fontaine, L. Gengembre, M. Traisnel, O. Lerasle, and N. Genet, Corrosion protection of galvanized steel and electroplating steel by decanoïc acid in aqueous solution: Electrochemical impedance spectroscopy, XPS and ATR-FTIR, *Corros. Sci.*, 51(2009), No. 6, p. 1201.